UCRL-JC-122340
PREPRINT
CONF-951182--7

2D Radiation-Magnetohydrodynamic Simulations of SATURN Imploding Z-Pinches

J. H. Hammer, J. L. Eddleman, P. T. Springer,
M. Tabak, A Toor, K. L. Wong, G. B. Zimmerman,
R. Humphreys, T. W. L. Sanford, and J. S. DeGroot

This paper was prepared for submittal to the
37th Annual Meeting of the American Physical Society
Division of Plasma Physics
Louisville, KY
November 6-10, 1995

November 6, 1995

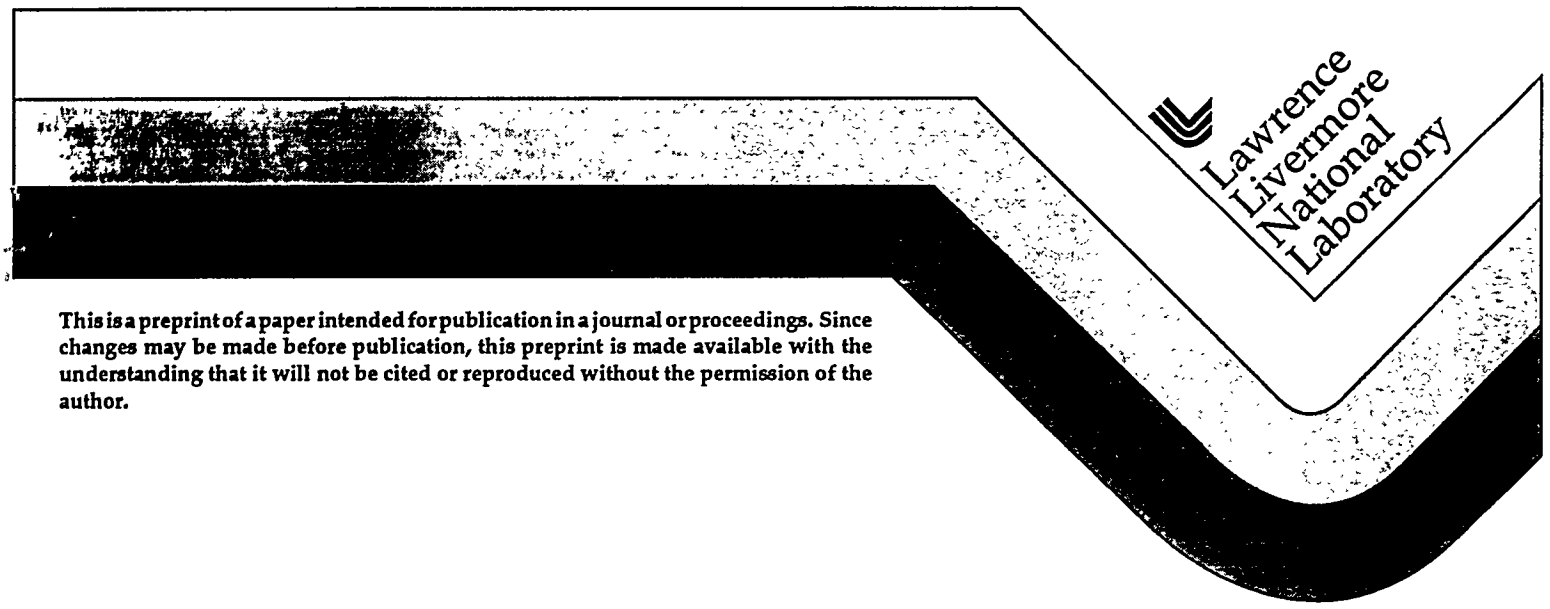

2D radiation-magnetohydrodynamic simulations of SATURN imploding z-pinches

James H. Hammer, James L. Eddleman, Paul T. Springer, Max Tabak,
Arthur Toor, Keith L. Wong and George B. Zimmerman
Lawrence Livermore National Laboratory, Livermore CA 94526

Russ Humphreys and Thomas W.L. Sanford
Sandia National Laboratory, Albuquerque, NM 87185

John S. DeGroot
University of California, Davis, CA 95616

ABSTRACT: Z-pinch implosions driven by the SATURN device at Sandia National Laboratory are modeled with a 2D radiation magnetohydrodynamic (MHD) code, showing strong growth of magneto-Rayleigh Taylor (MRT) instability. Modeling of the linear and nonlinear development of MRT modes predicts growth of bubble-spike structures that increase the time span of stagnation and the resulting x-ray pulse width. Radiation is important in the pinch dynamics. keeping the sheath relatively cool during the run-in and releasing most of the stagnation energy. The calculations give x-ray pulse widths and magnitudes in reasonable agreement with experiments, but predict a radiating region that is too dense and radially localized at stagnation. We also consider peaked initial density profiles with constant imploding sheath velocity that should reduce MRT instability and improve performance. 2D krypton simulations show an output x-ray power > 80 TW for the peaked profile.

PACS 52.30.-q, 52.30.Jb, 52.55.Ez

In section III we discuss MRT calculations using a 2D radiation-resistive magnetohydrodynamics (MHD) code developed at Lawrence Livermore National Laboratory and compare with experiments. We use the 2D code to follow the linear and non-linear development through the stagnation phase for different loads (aluminum wire arrays and solid-puff neon-argon implosions) . The 2D results differ strongly from 1D simulations. 1D calculations[5] typically show collapse of the entire mass of the pinch to a radius of 10's of microns and x-ray bursts of extreme power (~ several 100 TW for SATURN) and short duration (< 1 ns), while experiments show pinch radii of order several hundred microns, powers up to 30 TW and pulse times of 4 - 30 ns. The 2D simulations for most loads show strong MRT growth, causing the formation of bubbles and spikes from initial density perturbations of order 10^{-2}. The spikes contain most of the mass and become extended over a significant fraction of the initial radius. The radially-distributed mass stagnates and converts kinetic energy to x-rays over a much longer period than in 1D, in agreement with the experiment and as put forward by Husse, *et.al.*[6], on a heuristic basis. Direct evidence for the growth of MRT modes on SATURN can be found in recent experiments on neon-argon gas puff implosions that are sufficiently self-luminous to observe sheath structure during the implosion phase[2]. Earlier experiments also showed evidence of MRT mode growth[7,8].

in space and in the 20 to 30 eV range during the run-in phase. These conditions apply for many different materials and for most annular loads where ohmic heating is the dominant heating source and radiation keeps the plasma relatively cool. As a consequence, the plasma $\beta = 8\pi P/B^2$ is much smaller than 1. Fairly low Z, solid puff pinches, such as the neon-argon gas puff experiments, behave differently due to strong shock heating as the current sheet sweeps through the gas and can have $\beta \sim 1$.

Husse and Roderick[11] derived density profiles for a thin annular plasma accelerated by a magnetic field. They showed that the profile has two characteristic scales, $\Delta = \sqrt{\eta t}$ (we use resistivity units such that η is the magnetic diffusivity, i.e. $\eta \rightarrow \frac{\eta c^2}{4\pi}$ in Gaussian units) and $\delta = \frac{c_s^2}{g}$, with c_s the sound speed and acceleration, g. The profile is sketched in Fig.(2).

Typically, $\delta << \Delta$ for SATURN annular implosions. We can estimate the ratio of scales from force balance: $\rho \Delta g \approx \frac{B^2}{8\pi}$. so $\frac{\Delta}{\delta} \approx \frac{B^2}{8\pi\rho c_s^2} = \frac{1}{\beta} >> 1$. We exploit this separation of spatial scales in the following to derive an approximate linear theory.

Defining $x = r_{sheath} - r$, and assuming $\delta, \Delta << r_{sheath}$, we can write the MHD equilibrium equation in an accelerated reference frame:

order to make use of the analytic equilibrium in Eq. (2), we are also restricted to $k\Delta > 1$. Longer wavelength modes in the nonlinear regime are ultimately the most destructive[4], but these are fed by the cascade from shorter wavelengths as we see in the 2D simulations.

The linearized resistive MHD equations are given by

$$\begin{aligned}
&\rho_1 = \nabla \bullet \rho\vec{\xi} \\
&\rho\frac{\partial^2\vec{\xi}}{\partial t^2} + \rho_1 g = -\nabla\left(P_1 + BB_1\right) \\
&\frac{\partial\vec{B}_1}{\partial t} = \nabla\times\left(\frac{\partial\vec{\xi}}{\partial t}\times\vec{B}\right) + \eta\nabla^2\vec{B}_1 \\
&P_1 = \rho_1 c_s^2
\end{aligned} \tag{3}$$

We have assumed uniform resistivity and an isothermal equation of state for the perturbations. Using $\rho_1, \vec{\xi}, B_1 \propto e^{ikz+\int\gamma dt}$, we can algebraically eliminate ρ_1 and ξ_{1z}. The equations are further simplified by the approximation $\frac{\gamma^2}{k^2 v_{Alfven}^2} << 1$, $v_{Alfven}^2 = \frac{B^2}{4\pi\rho}$. This is consistent with the earlier approximations since if $\gamma \approx \sqrt{kg}$ then $\frac{\gamma^2}{k^2 v_{Alfven}^2} \approx \frac{g}{k v_{Alfven}^2} \approx \frac{1}{k\Delta}$.

The resulting equations are:

B-field is nearly uniform for x<<Δ. Nearly-incompressible perturbations then produce very little perturbed B or current density, and the resistivity has comparatively little effect. Longer wavelength modes that sample more of the sheath and gradients in magnetic field may have resistive effects entering[4] when $\gamma \approx \eta k^2$. For the general case, the equations can be put in dimensionless form with eigenvalue γ/γ_0, where $\gamma_0 = \frac{g}{c_s}$. γ/γ_0 is a function of only two parameters, kδ and $\mu \equiv \frac{\eta g}{v_A^2 c_s}$. The evaluation of $\gamma/\gamma_0 (k\delta,\mu)$ is left to a future publication.

III. 2D RADIATION MAGNETOHYDRODYNAMIC MODELING

The 2D radiation MHD code used for this modeling solves the MHD continuity, momentum, energy and magnetic field equations in axisymmetric r-z geometry. Radiation is transported by a multigroup diffusion model with frequency-dependent emissivity and opacity determined by an average atom treatment[12]. These simulations employ an analytic equation of state based on the Thomas-Fermi-Cowan model[13]. The magnetic field, assumed to be purely azimuthal, evolves due to advection, magnetic diffusion and the action of the Nernst term. Only classical

constant z (K-lines) and lines of constant r (L-lines) distributed so as to resolve the initial density distribution. As the problem evolves, we rezone the mesh each cycle to restore straight, constant-z K-lines and either a) allow the L-lines to follow the radial portion of the Lagrangian flow, except where the mesh collapses below a minimum zone size, or b) keep the L-lines straight but move the finely-resolved region with the center-of-mass motion of the plasma. Techniques a) and b) give us finer radial resolution than a completely Eulerian calculation for a given number of zones, and are less subject to numerical diffusion as plasma flows across the mesh during the implosion.

Several different load geometries and materials have been modeled. In most cases we model only a fraction of the pinch length, e.g., 1/10th or 1/5th, in order to resolve the mode structure with a moderate number of zones ($15<k_{max}<201$ for the calculations shown). We impose either zero-derivative axial boundary conditions, for 1/2 wavelength, single mode problems or periodic axial boundary conditions for multimode simulations. The plasma is initially perturbed with a density fluctuation varying axially as $\cos(\pi z/z_{max})$ and radially as the unperturbed distribution in the 1/2 wavelength case, or with a random zone-to-zone density fluctuation for the multimode case. Initial perturbations of order 1% are usually enough to induce strong MRT activity. Since the initial density distributions for

Simulations with larger initial amplitude (~10^{-2} density perturbation) develop nonlinear behavior after imploding to .75 x initial radius. Large bubble-spike structures develop and by the time the bubbles reach the symmetry axis, the spike tips are at .3 - .5 x initial radius. In multimode calculations, short wavelengths that appear early in time are gradually replaced by longer scale-length structures as seen in hydrodynamic RT modeling. The radial smearing of the mass from the breakup into bubble-spikes sets the time scale for the stagnation on axis to $t_{stag} = t_{spike} - t_{bubble}$ where t_{spike}, t_{bubble} are the arrival times for the spike tip and bubble, respectively[6]. Since the radiation is produced when kinetic energy is converted to thermal energy, the output radiation pulse also occurs in a time of order t_{stag}. Fig.(3) shows the calculated output power for three different simulations in comparison with the bolometer signal from shot 2094. The only free parameters in the calculations are the initial amplitude, for the single mode and multimode calculations, and wavelength, for the single mode calculation. Large variations in the initial conditions produce only factor of 2 variations in the output radiation pulse, suggesting that the nonlinear development is fairly insensitive to the initial perturbation.

The code does not agree with the spatial extent of the radiating region near r=0. For shot 2094, the spatial FWHM of the keV x-ray emission observed with a framing camera reaches a minimum of 600 μm, at t=81 ns, while postprocessing of simulation C in Fig.(3) gives a FWHM

B. Neon-argon gas puff simulations

Recent experiments on neon-argon implosions have the advantage of increased luminosity of the sheath during the run-in phase, which reveals some of the structure of the unstable sheath. Fig. (4) shows a keV x-ray framing picture of an implosion 3 ns before stagnation. The distortion of the sheath is consistent with MRT growth at wavelengths ~ mm.

The code predicts high temperatures (few hundred eV) and x-ray emission during the run-in due to shock heating of the gas, as opposed to ~30 eV for narrow, annular loads that are mostly ohmically heated. Also, the density and average Z of the plasma are low enough to limit the total radiative cooling (these cases are much brighter in keV radiation than annular loads, however, as seen in the experiment). 2D runs show the development of the familiar bubble-spike structure, as shown in Fig.(5). This simulation models 0.4 cm of the 2 cm total pinch length, with an approximately uniform initial distribution of argon and neon (50% atomic fraction of each) out to a radius of 2.25 cm, with 100 μg/cm mass, 1% initial random density perturbation and periodic boundary conditions in z. The mass clumps shown in Fig. (5) appear as axisymmetric rings of emission when viewed externally. Fig. (6) shows a post-processed image of the simulation at the same point in the implosion (about midway) as Fig. (5). To generate the image, we integrate the radiation transport equation

imploding plasma, reducing the assembled power density and increasing the stagnation/x-ray output time. The possible benefits from reducing the instability could be power amplification, $P_{x\text{-}ray} >> P_{drive}$, higher stagnation density for improved high-Z K-shell yield, improved control of plasma parameters for high energy density experiments and better ability to model and predict performance for existing and future devices.

One potential method for reducing MRT growth is to adjust the initial density distribution so that the unstable interface between the plasma and magnetic field has reduced (or zero) acceleration. For a radially-extended initial density profile, i.e., not a narrow annular shell, the current sheet "snow plows" through the gas. For high enough Z, the sheath remains cool and narrow due to radiation and accretes mass as it implodes. The reduced MRT drive comes at the cost of losing approximately 50% of the sheath kinetic energy to radiation during the run-in.

We can use simple OD force balance arguments to derive the shape of a profile with constant implosion velocity. The force equation gives

$$\frac{L'I^2}{2} = \dot{M}v \qquad (6)$$

where $L' = \frac{\mu_0}{2\pi}\frac{l}{r}$ is the radial rate-of-change of the inductance and $\dot{M} = 2\pi l \rho v$ is the mass snowplow rate. Given a current versus time we can solve Eq.(6) for the density:

boundary conditions modeling 1/10 of a total pinch length of 2 cm. The implosion still shows significant 2D behavior, possibly as a result of residual curvature-driven instability or Richtmeyer-Meshkov instability of the snowplow shock front. A slight deceleration of the sheath might compensate for the curvature driven instability. The simulation output power is enhanced, however, in comparison with experiments or 2D modeling of annular loads. The output power exceeds 80 TW with 30 TW greater than 1 keV, as shown in Fig.(9).

A possible method for generating these profiles is to embed a solid wire in a gas puff peaked on axis. The wire will heat and expand under the influence of the x-rays produced during the sheath run-in, creating a profile resembling Fig.(8). Also, deviations from the profile within a radius ~ mm will probably not degrade performance appreciably.

V. CONCLUSIONS

2D radiation MHD calculations indicate that MRT modes should grow to large amplitude and determine the x-ray output pulse widths for a variety of SATURN loads. The code predicts x-ray output times and magnitudes in approximate agreement with experiments, although the simulations over-predict the density near r = 0. Relatively weak 3D effects could reduce the peak density significantly since the mass near the origin has undergone a large radial convergence, although anomalous resistance

[3] T.W.L. Sanford, T.J. Nash, B.M. Marder, R. Humphreys, C. Deeney, R.B. Spielman, J.F. Seamen, R.C. Mock, J.S. McGurn, D. Jobe, T.L. Gilliland, M. Vargas, K. Struve, W.A. Stygar, J.H. Hammer, J.L. Eddleman, J.S. DeGroot, D. Mosher, K.G. Whitney, J.P. Apruzese, P. Pulsifer, Y. Maron, Bull. Am. Phys. Soc., 8R02,(1995).

[4] T.W. Hussey, N.F. Roderick, and D.A. Kloc, J. Appl. Phys. **51**,1452 (1980).

[5] J.H. Hammer,J.L Eddleman, J.S. DeGroot, M. Tabak, A. Toor and G.B. Zimmerman,Bull. Am. Phys. Soc. (1994).

[6] T.W. Hussey, N.F. Roderick, U. Shumlak, R.B. Spielman and C.Deeney, Phys. Plasmas **2**,2055(1995).

[7] R.B. Spielman, D.L. Hanson, M.A. Palmer, M.K. Matzen, T.W. Hussey, and J.M. Peek, J. Appl. Phys. **57**, 883 (1985).

[8] W.Hsing (private communication, 1989).

[9] J.L. Eddleman, J.S. DeGroot, R.B. Spielman, C.W. Hartman. M.Gee, J.H. Hammer,K.G. Estabrook, W.B. Bateson and D.W. Hewett, Bull. Am. Phys. Soc. ,8R13 (1995)

[10] N.F. Roderick and T.W. Hussey, J. Appl. Phys. **56**, 1387 (1984).

[11] T.W. Husse and N.F. Roderick, Phys. Fluids **24**,1384 (1981).

FIGURE CAPTIONS

Fig.(1) Imploding z-pinch configuration.

Fig.(2) Density profile in an accelerated reference frame.

Fig.(3) X-ray output power per unit solid angle measured by the bolometer for shot 2094 in TW/sr, compared with simulations: A, a single mode density perturbation with amplitude 1% and wavelength 1 mm; B, a 1% random initial density perturbation with periodic boundary conditions and simulation length of 2 mm; C, a 5% random density perturbation with periodic boundary conditions and simulation length of 1 mm.

Fig.(4) X-ray framing camera image (width at source = 1.2 cm) of an imploding neon-argon solid gas puff 3 ns before stagnation. The z-axis is vertical and the view angle is 65° from the z-axis. The shadow of the anode wires is visible.

Fig.(5) Density contours from a simulation of neon-argon gas puff at t = 67 ns. The peak value is 3.2×10^{-4} g/cc. The initial puff density is 9×10^{-6} g/cc.

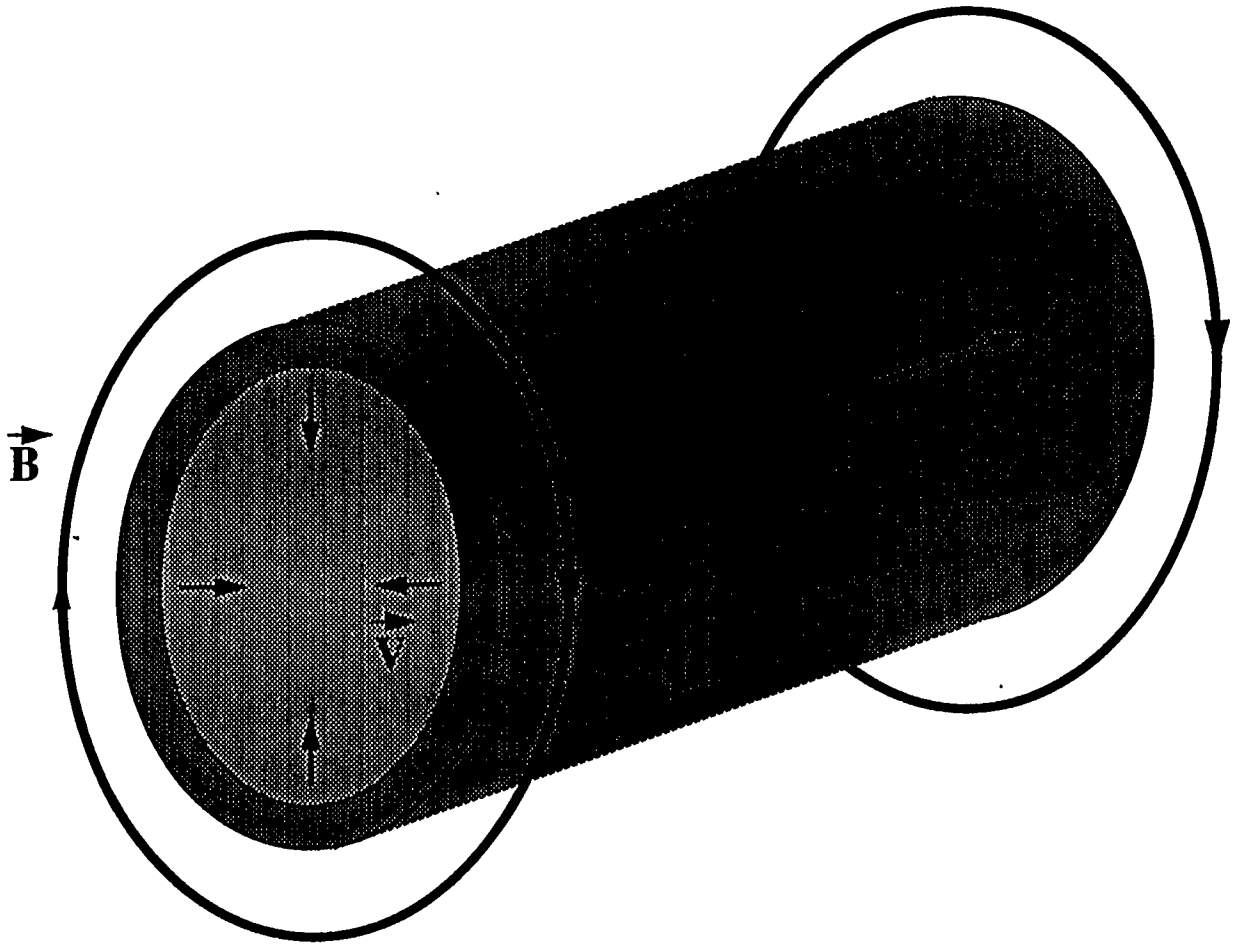

Fig. 1, Hammer,et.al., Phys. Plasmas

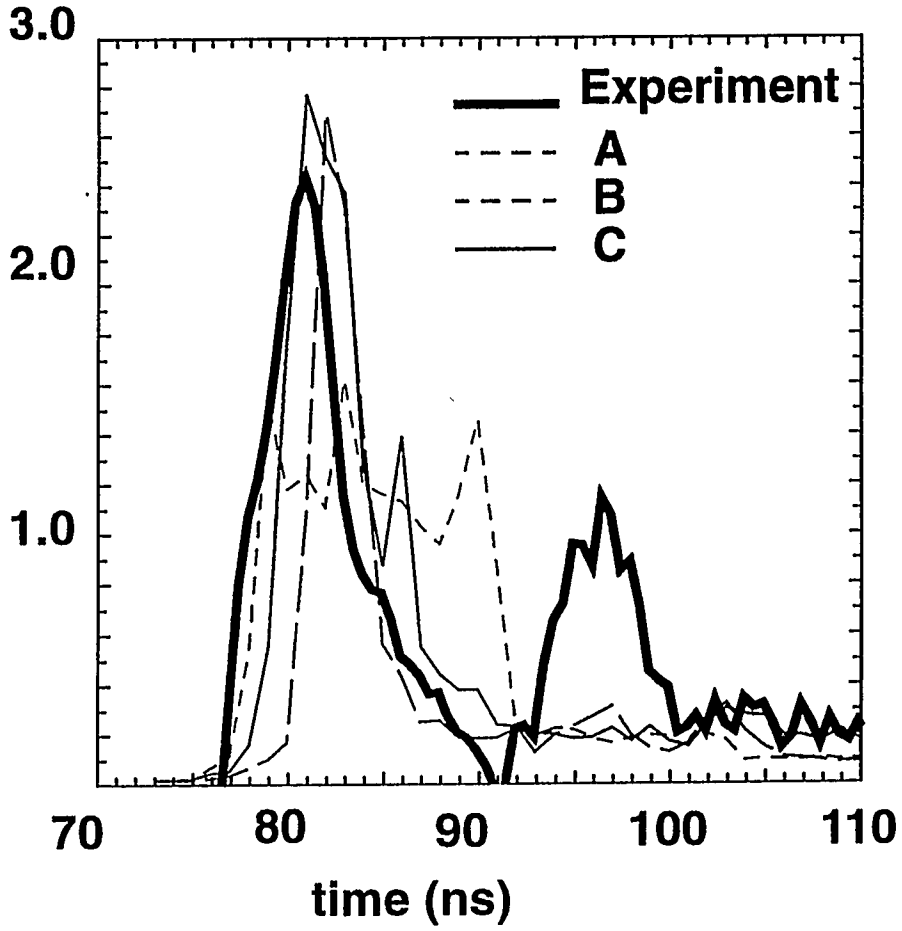

Fig. 3, Hammer, et.al., Phys. Plasmas

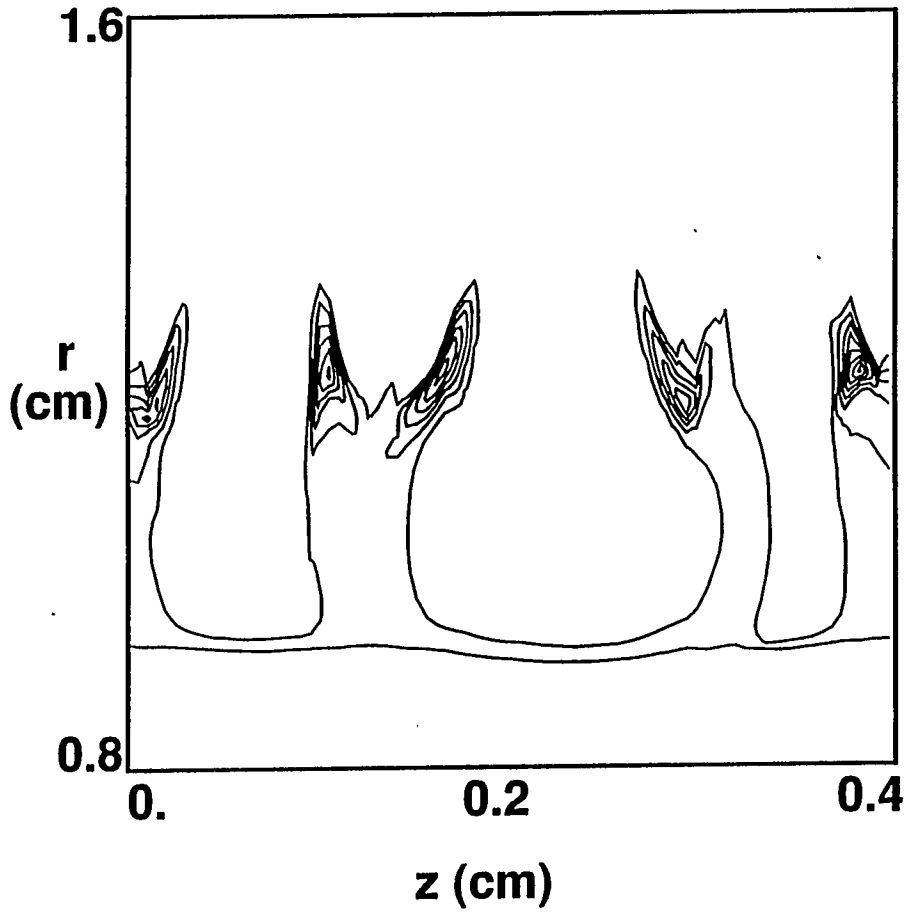

Fig. 5, Hammer, et. al., Phys. Plasmas

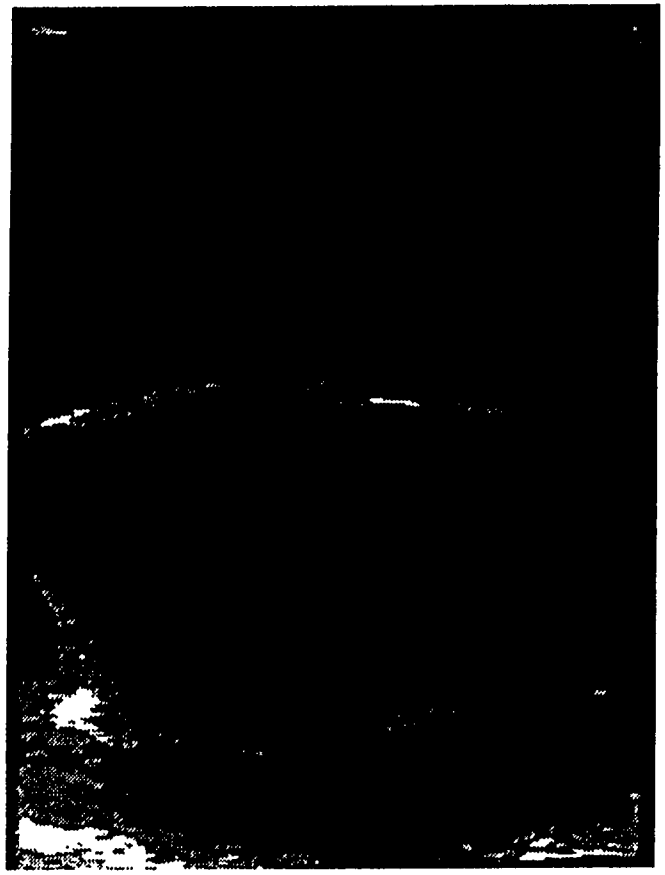

Fig. 7, Hammer,et.al., Phys. Plasmas

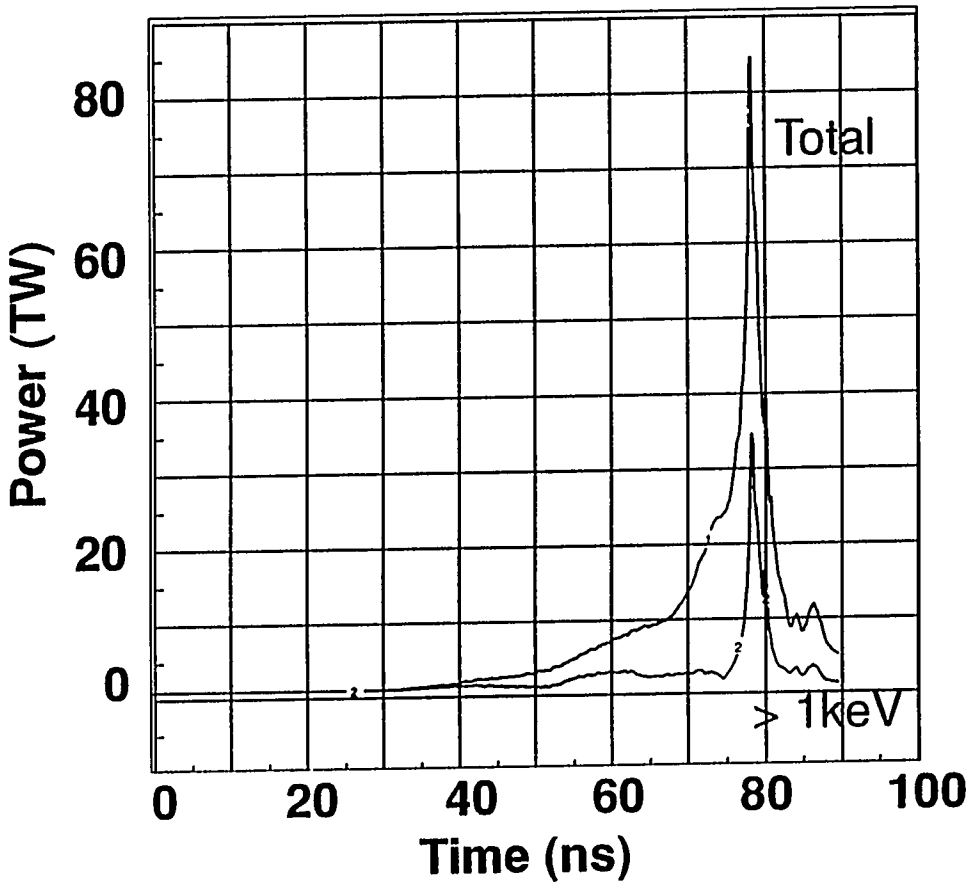

Fig. 9 Hammer et al. Phys. Plasmas

UCRL-JC-122340
PREPRINT
CONF-951182--7

2D Radiation-Magnetohydrodynamic Simulations of SATURN Imploding Z-Pinches

J. H. Hammer, J. L. Eddleman, P. T. Springer,
M. Tabak, A Toor, K. L. Wong, G. B. Zimmerman,
R. Humphreys, T. W. L. Sanford, and J. S. DeGroot

This paper was prepared for submittal to the
37th Annual Meeting of the American Physical Society
Division of Plasma Physics
Louisville, KY
November 6-10, 1995

November 6, 1995

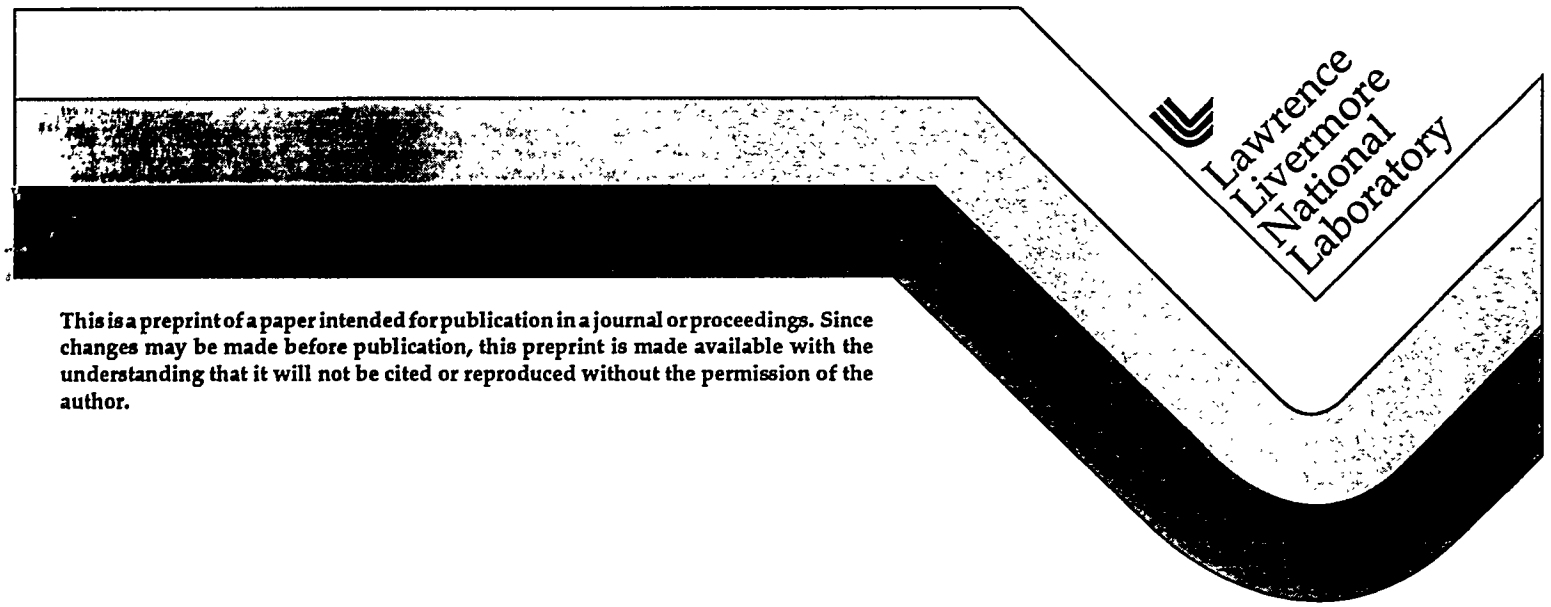

2D radiation-magnetohydrodynamic simulations of SATURN imploding z-pinches

James H. Hammer, James L. Eddleman, Paul T. Springer, Max Tabak,
Arthur Toor, Keith L. Wong and George B. Zimmerman
Lawrence Livermore National Laboratory, Livermore CA 94526

Russ Humphreys and Thomas W.L. Sanford
Sandia National Laboratory, Albuquerque, NM 87185

John S. DeGroot
University of California, Davis, CA 95616

ABSTRACT: Z-pinch implosions driven by the SATURN device at Sandia National Laboratory are modeled with a 2D radiation magnetohydrodynamic (MHD) code, showing strong growth of magneto-Rayleigh Taylor (MRT) instability. Modeling of the linear and nonlinear development of MRT modes predicts growth of bubble-spike structures that increase the time span of stagnation and the resulting x-ray pulse width. Radiation is important in the pinch dynamics. keeping the sheath relatively cool during the run-in and releasing most of the stagnation energy. The calculations give x-ray pulse widths and magnitudes in reasonable agreement with experiments, but predict a radiating region that is too dense and radially localized at stagnation. We also consider peaked initial density profiles with constant imploding sheath velocity that should reduce MRT instability and improve performance. 2D krypton simulations show an output x-ray power > 80 TW for the peaked profile.

PACS 52.30.-q, 52.30.Jb, 52.55.Ez

I. INTRODUCTION

Imploding z-pinches employing gas puffs, wire arrays or cylindrical foils are of interest as intense sources of keV x-rays for nuclear weapons effects and sources of thermal x-rays for high energy density physics experiments[1]. Developing an understanding of the detailed pinch dynamics is critical for predicting scaling, optimizing performance and for designing loads that reach desired plasma and radiation field conditions. In this paper we describe radiation-magnetohydrodynamic (MHD) code modeling of pinches driven by the SATURN pulse power device at Sandia National Laboratory[1] and compare to the experiments[2,3]. The simplest pinch geometry, consisting of a plasma annulus, is sketched in Fig. (1). SATURN drives imploding pinch loads at currents up to 10 MA, with a rise time of about 50 ns and peak electrical power of 15 TW.

Instability of the imploding plasma with respect to magneto-Rayleigh Taylor (MRT) modes[4] has been predicted to alter the implosion dynamics profoundly and is the focus of this paper. In section II we derive approximate linearized equations for the instability, making use of the separation of spatial scales that occurs for a radiatively-cooled plasma as predicted for SATURN. The growth rate can be found analytically in some limits, showing the stabilizing effect of resistivity on short wavelength modes.

In section III we discuss MRT calculations using a 2D radiation-resistive magnetohydrodynamics (MHD) code developed at Lawrence Livermore National Laboratory and compare with experiments. We use the 2D code to follow the linear and non-linear development through the stagnation phase for different loads (aluminum wire arrays and solid-puff neon-argon implosions) . The 2D results differ strongly from 1D simulations. 1D calculations[5] typically show collapse of the entire mass of the pinch to a radius of 10's of microns and x-ray bursts of extreme power (~ several 100 TW for SATURN) and short duration (< 1 ns), while experiments show pinch radii of order several hundred microns, powers up to 30 TW and pulse times of 4 - 30 ns. The 2D simulations for most loads show strong MRT growth, causing the formation of bubbles and spikes from initial density perturbations of order 10^{-2}. The spikes contain most of the mass and become extended over a significant fraction of the initial radius. The radially-distributed mass stagnates and converts kinetic energy to x-rays over a much longer period than in 1D. in agreement with the experiment and as put forward by Husse, *et.al.*[6], on a heuristic basis. Direct evidence for the growth of MRT modes on SATURN can be found in recent experiments on neon-argon gas puff implosions that are sufficiently self-luminous to observe sheath structure during the implosion phase[2]. Earlier experiments also showed evidence of MRT mode growth[7,8].

An important difference between 2D modeling and experiment is the lower peak density and broader emission region experimentally observed at stagnation[3]. We conjecture that, while the gross dynamics during the implosion phase appear to be reproduced in 2D modeling, a relatively small amount of 3 dimensional variation may explain the reduced stagnation density. Alternative possibilities include deviations from the classical resistivity model employed by the code[9], which could affect both the linear growth rates and nonlinear saturation[10] , rapid sub-grid scale mixing or the Hall effect and other terms dropped from the MHD ordering.

Given the evidence for strong MRT instability, we are exploring ways to reduce its growth and improve performance and our ability to model pinch behavior. One approach is to vary the pinch initial conditions so that the sheath is subjected to less acceleration. As we discuss in section IV, there are initial density profiles that result in zero sheath acceleration which, in principal, remove MRT instability. 2D simulations show residual instability but with significant reduction of the mass spreading that degrades performance for most loads.

II. ANALYTIC MAGNETO-RAYLEIGH TAYLOR MODELING

From 1 and 2D radiation-MHD modeling of SATURN pinches we find that the bulk electron and ion temperatures are approximately uniform

in space and in the 20 to 30 eV range during the run-in phase. These conditions apply for many different materials and for most annular loads where ohmic heating is the dominant heating source and radiation keeps the plasma relatively cool. As a consequence, the plasma $\beta = 8\pi P/B^2$ is much smaller than 1. Fairly low Z, solid puff pinches, such as the neon-argon gas puff experiments, behave differently due to strong shock heating as the current sheet sweeps through the gas and can have $\beta \sim 1$.

Husse and Roderick[11] derived density profiles for a thin annular plasma accelerated by a magnetic field. They showed that the profile has two characteristic scales, $\Delta = \sqrt{\eta t}$ (we use resistivity units such that η is the magnetic diffusivity, i.e. $\eta \rightarrow \frac{\eta c^2}{4\pi}$ in Gaussian units) and $\delta = \frac{c_s^2}{g}$, with c_s the sound speed and acceleration, g. The profile is sketched in Fig.(2).

Typically, $\delta << \Delta$ for SATURN annular implosions. We can estimate the ratio of scales from force balance: $\rho \Delta g \approx \frac{B^2}{8\pi}$. so $\frac{\Delta}{\delta} \approx \frac{B^2}{8\pi\rho c_s^2} = \frac{1}{\beta} >> 1$. We exploit this separation of spatial scales in the following to derive an approximate linear theory.

Defining $x = r_{sheath} - r$, and assuming $\delta, \Delta << r_{sheath}$, we can write the MHD equilibrium equation in an accelerated reference frame:

$$\rho g = -\frac{\partial}{\partial x}\left(P + \frac{B^2}{8\pi}\right) \qquad (1)$$

For simplicity, and in rough accord with the 1 and 2D simulations, we assume constant temperature so the pressure is given by $P = \rho c_s^2$, with c_s^2 a constant. For scales much shorter than the resistive skin depth, Δ, the current density will be uniform, $\partial B / \partial x = const.$ Assuming β <<1, we can then solve Eq. 1 for the density profile,

$$\rho = \rho_0 \left(1 - e^{-x/\delta}\right) \qquad (2)$$

This solution shows the density rise at the outer portion of the sheath depicted in Figure 2. This is the interesting (unstable) region from the point of view of MRT instability.

Next we consider linear stability of the accelerated equilibrium. We expect growth rates, $\gamma \approx \sqrt{kg}$,for perturbations varying as e^{-kz}. Azimuthal symmetry is assumed for the modes since non-symmetric modes are (at least partially) stabilized by field line bending. Since $g \approx r_{sheath} / t_{implosion}^2$, and restricting to $kr_{sheath} >> 1$, we have $\gamma t_{implosion} \approx \sqrt{kr_{sheath}} >> 1$. Since the growth rate is large compared to the rate of change of equilibrium quantities we can assume perturbations vary as $e^{\int \gamma dt}$ with γ calculated from the instantaneous linearized equations. In

order to make use of the analytic equilibrium in Eq. (2), we are also restricted to $k\Delta > 1$. Longer wavelength modes in the nonlinear regime are ultimately the most destructive[4], but these are fed by the cascade from shorter wavelengths as we see in the 2D simulations.

The linearized resistive MHD equations are given by

$$\begin{aligned}
&\rho_1 = \nabla \bullet \rho\vec{\xi} \\
&\rho\frac{\partial^2\vec{\xi}}{\partial t^2} + \rho_1 g = -\nabla\left(P_1 + BB_1\right) \\
&\frac{\partial\vec{B}_1}{\partial t} = \nabla\times\left(\frac{\partial\vec{\xi}}{\partial t}\times\vec{B}\right) + \eta\nabla^2\vec{B}_1 \\
&P_1 = \rho_1 c_s^2
\end{aligned} \tag{3}$$

We have assumed uniform resistivity and an isothermal equation of state for the perturbations. Using $\rho_1, \vec{\xi}, B_1 \propto e^{ikz+\int\gamma dt}$, we can algebraically eliminate ρ_1 and ξ_{1z}. The equations are further simplified by the approximation $\frac{\gamma^2}{k^2 v_{Alfven}^2} << 1$, $v_{Alfven}^2 = \frac{B^2}{4\pi\rho}$. This is consistent with the earlier approximations since if $\gamma \approx \sqrt{kg}$ then $\frac{\gamma^2}{k^2 v_{Alfven}^2} \approx \frac{g}{k v_{Alfven}^2} \approx \frac{1}{k\Delta}$.

The resulting equations are:

$$-\gamma^2\rho\xi + \rho' g\xi - g\frac{\rho}{B}RB_1 = -\frac{\gamma^2}{k^2}\left(\rho\xi' + \frac{\rho}{B}RB_1\right)'$$

$$B_1 + \left(\frac{c_s^2}{v_A^2} + \frac{\gamma^2}{k^2}\right)RB_1 = \frac{\gamma^2}{k^2 v_A^2}\xi' B + \frac{\xi\rho' c_s^2}{B} \qquad (4)$$

where $\xi = \vec{\xi}_x$, $RB_1 = -\frac{\eta}{\gamma}\left(\frac{\partial^2}{\partial x^2} - k^2\right)B_1$, $(\,)' = \frac{\partial}{\partial x}(\,)$, and $v_A^2 = B^2/4\pi\rho$.

The boundary conditions are $\xi = 1, B_1 = 0$ at $x = 0$ and $\xi, B_1 \to 0$ as $x \to \infty$.

One interesting limit is the zero resistivity case where the equations reduce to the standard incompressible eigenvalue equation for RT instability. For the profile given in Eq. (2), the largest eigenvalue can be found analytically and is given exactly by $\gamma = \sqrt{kg}$ with solution $\xi = e^{-kx}$. The maximum growth rate does not saturate at large k, as found for most diffuse profiles, where $\gamma = \sqrt{g\frac{\rho'}{\rho}}$ since $\frac{\rho'}{\rho} \to \infty$ as x goes to 0. For finite η, and $k\delta >> 1$, we can find a local dispersion relation,

$$\gamma = \sqrt{\frac{\rho'}{\rho}g + \left(\frac{\eta k^2}{2}\frac{c_s^2}{v_A^2}\right)^2} - \frac{\eta k^2}{2}\frac{c_s^2}{v_A^2} \qquad (5)$$

From Eq.(5) we see that high k modes are resistively stabilized, although less effectively than from the estimate $\gamma \approx \eta k^2$ by a factor of $c_s^2/v_A^2 = \beta/2 << 1$. This factor is present because at low β, the equilibrium

B-field is nearly uniform for x<<Δ. Nearly-incompressible perturbations then produce very little perturbed B or current density, and the resistivity has comparatively little effect. Longer wavelength modes that sample more of the sheath and gradients in magnetic field may have resistive effects entering[4] when $\gamma \approx \eta k^2$. For the general case, the equations can be put in dimensionless form with eigenvalue γ/γ_0, where $\gamma_0 = \frac{g}{c_s}$. γ/γ_0 is a function of only two parameters, kδ and $\mu \equiv \frac{\eta g}{v_A^2 c_s}$. The evaluation of $\gamma/\gamma_0 (k\delta,\mu)$ is left to a future publication.

III. 2D RADIATION MAGNETOHYDRODYNAMIC MODELING

The 2D radiation MHD code used for this modeling solves the MHD continuity, momentum, energy and magnetic field equations in axisymmetric r-z geometry. Radiation is transported by a multigroup diffusion model with frequency-dependent emissivity and opacity determined by an average atom treatment[12]. These simulations employ an analytic equation of state based on the Thomas-Fermi-Cowan model[13]. The magnetic field, assumed to be purely azimuthal, evolves due to advection, magnetic diffusion and the action of the Nernst term. Only classical

collisional effects based on the Lee and More extension of Spitzer resistivity are included[14]. The Hall effect and similar terms usually neglected in the MHD ordering are not included in this work, but will be in future calculations.

The magnetic field is coupled self consistently to an external circuit through a "circuit region" at the outer edge of the calculation, contiguous with the plasma region. The circuit region is treated as an insulator with magnetic field determined by the external circuit current. The loop voltage around the circuit region, treating the boundaries as conductors but using the self-consistent electric field at the plasma edge, is placed in series with the external circuit. The external circuit can consist of a resistor, inductor, capacitor and programmed voltage source in series with the plasma load. For the SATURN simulations we use a programmed voltage source in series with a 1/6 Ω resistor to model the known output of the pulse-forming line, and an inductor to account for the power feed region near the pinch.

The code is Lagrangian on a logically-rectangular mesh with indices K,L. Due to large distortions and tangling of the mesh in the presence of strong MRT modes, we make use of the rezoning capability of the code. The rezoner employs Van Leer corrections for second order accuracy when gradients are well resolved. Several variations on rezoning schemes have been tested. Typically the initial mesh has evenly-spaced lines of

constant z (K-lines) and lines of constant r (L-lines) distributed so as to resolve the initial density distribution. As the problem evolves, we rezone the mesh each cycle to restore straight, constant-z K-lines and either a) allow the L-lines to follow the radial portion of the Lagrangian flow, except where the mesh collapses below a minimum zone size, or b) keep the L-lines straight but move the finely-resolved region with the center-of-mass motion of the plasma. Techniques a) and b) give us finer radial resolution than a completely Eulerian calculation for a given number of zones, and are less subject to numerical diffusion as plasma flows across the mesh during the implosion.

Several different load geometries and materials have been modeled. In most cases we model only a fraction of the pinch length, e.g., 1/10th or 1/5th, in order to resolve the mode structure with a moderate number of zones ($15<k_{max}<201$ for the calculations shown). We impose either zero-derivative axial boundary conditions, for 1/2 wavelength, single mode problems or periodic axial boundary conditions for multimode simulations. The plasma is initially perturbed with a density fluctuation varying axially as $\cos(\pi z/z_{max})$ and radially as the unperturbed distribution in the 1/2 wavelength case, or with a random zone-to-zone density fluctuation for the multimode case. Initial perturbations of order 1% are usually enough to induce strong MRT activity. Since the initial density distributions for

SATURN loads have not been characterized to the few percent level, we test the sensitivity of the results to variation in the initial amplitude.

A. Aluminum wire array simulations

The aluminum wire-array simulations are for an array with radius = 0.86 cm, length = 2.0 cm and 328 μg/cm mass[3]. The calculations are done for fractions of the pinch length varying from .05 to .5. We initiate the calculations with a gaussian mass distribution with a FWHM of 0.13 cm and temperature of 1 eV, modeling the conditions of the wire array following the SATURN prepulse of 50-100 kA for 100 ns (single wire calculations with a model prepulse were used to predict these initial conditions). The expanded profile of individual wires due to the prepulse should significantly overlap neighboring wires for arrays with ≈ 90 wires, providing some justification for ignoring the azimuthal structure. We employed simulations with small initial density perturbations ($\sim 10^{-5}$) to study linear-phase growth. These confirm that modes with a wavelength ~ 1 mm have growth rates ~ $\sqrt{kg}$, while at shorter wavelengths the growth rate increases less rapidly and saturates or drops for wavelengths < 10^{-2} cm, as expected from resistive effects. The growth rate varies less than a factor of 2 for wavelengths between 10^{-2} - 10^{-1} cm.

Simulations with larger initial amplitude (~10^{-2} density perturbation) develop nonlinear behavior after imploding to .75 x initial radius. Large bubble-spike structures develop and by the time the bubbles reach the symmetry axis, the spike tips are at .3 - .5 x initial radius. In multimode calculations, short wavelengths that appear early in time are gradually replaced by longer scale-length structures as seen in hydrodynamic RT modeling. The radial smearing of the mass from the breakup into bubble-spikes sets the time scale for the stagnation on axis to $t_{stag} = t_{spike} - t_{bubble}$ where t_{spike}, t_{bubble} are the arrival times for the spike tip and bubble, respectively[6]. Since the radiation is produced when kinetic energy is converted to thermal energy, the output radiation pulse also occurs in a time of order t_{stag}. Fig.(3) shows the calculated output power for three different simulations in comparison with the bolometer signal from shot 2094. The only free parameters in the calculations are the initial amplitude, for the single mode and multimode calculations, and wavelength, for the single mode calculation. Large variations in the initial conditions produce only factor of 2 variations in the output radiation pulse, suggesting that the nonlinear development is fairly insensitive to the initial perturbation.

The code does not agree with the spatial extent of the radiating region near r=0. For shot 2094, the spatial FWHM of the keV x-ray emission observed with a framing camera reaches a minimum of 600 μm, at t=81 ns, while postprocessing of simulation C in Fig.(3) gives a FWHM

of 50 μm at the same time. In the simulation, the radiating region contains ~ 10 - 20% of the total mass in a region of very small size (~10's of μm) with the bulk of the material at scales of order 500 - 1000 μm. Radiation cooling plays an important role in allowing the convergence of part of the mass to high density, in analogy with the more extreme radiative collapse observed in 1D[5].

3D effects are a possible explanation for the discrepancy. A small breaking of azimuthal symmetry would have small effect on the run-in dynamics and MRT development, but could give imploding mass elements angular momentum that would prevent high convergence. Resistive effects may also play a role. The simulations show behavior late in the implosion similar to the saturation model of Roderick and Husse[10], where material from the spikes diffuses into the "throat" of a bubble and partially shorts out the accelerating current. The bubble throat develops flow similar to a MHD nozzle. Enhanced resistivity[9] would increase mass transport into the bubbles and may reduce the current density near r=0 that helps drive radiative collapse.

In addition, the Hall (and similar) terms may be important. The high aspect ratio, $\Delta r/\Delta z \sim 10$, of the bubble-spike structures could magnify the importance of the Hall effect, i.e., the small axial mass flow associated with the polarization drift may be sufficient to short out the bubbles.

B. Neon-argon gas puff simulations

Recent experiments on neon-argon implosions have the advantage of increased luminosity of the sheath during the run-in phase, which reveals some of the structure of the unstable sheath. Fig. (4) shows a keV x-ray framing picture of an implosion 3 ns before stagnation. The distortion of the sheath is consistent with MRT growth at wavelengths ~ mm.

The code predicts high temperatures (few hundred eV) and x-ray emission during the run-in due to shock heating of the gas, as opposed to ~30 eV for narrow, annular loads that are mostly ohmically heated. Also, the density and average Z of the plasma are low enough to limit the total radiative cooling (these cases are much brighter in keV radiation than annular loads, however, as seen in the experiment). 2D runs show the development of the familiar bubble-spike structure, as shown in Fig.(5). This simulation models 0.4 cm of the 2 cm total pinch length, with an approximately uniform initial distribution of argon and neon (50% atomic fraction of each) out to a radius of 2.25 cm, with 100 μg/cm mass, 1% initial random density perturbation and periodic boundary conditions in z. The mass clumps shown in Fig. (5) appear as axisymmetric rings of emission when viewed externally. Fig. (6) shows a post-processed image of the simulation at the same point in the implosion (about midway) as Fig. (5). To generate the image, we integrate the radiation transport equation

along rays parallel to the view angle of the Sandia Large Format framing camera (35° off normal) and filter the multi-photon-group output through the filters and response function of the camera. The off-normal view causes the emitting rings to appear as ellipses (clipped by the field of view), with the far side of the ellipse dimmed by opacity of the intervening gas. Fig. (6) shows a framing camera image from shot 2019 at a comparable point in the implosion, with a similar ring structure clearly visible. The observation of a single ring vs. several in the simulation may be due to hour-glassing of the implosion from axial nonuniformity that is not included in the model. The ring structures are commonly observed in the neon-argon data, and offer strong evidence that axisymmetric MRT activity is occurring.

In these experiments, the stagnation density was measured from Stark broadening of argon K-shell emission and found to be ~ 10^{-3} g/cc. As for the aluminum simulations, at any given point in time during stagnation, a small fraction of the mass is at high density ~ 10 g/cc in a very small volume, in disagreement with the experiment. The discussion in section III.A regarding effects that would disrupt the convergence applies here as well.

IV. IMPROVED STABILITY PROFILES

As we have seen in sections II and III, MRT instability appears to have severe effects on performance of the z-pinch, causing break-up of the

imploding plasma, reducing the assembled power density and increasing the stagnation/x-ray output time. The possible benefits from reducing the instability could be power amplification, $P_{x\text{-}ray} >> P_{drive}$, higher stagnation density for improved high-Z K-shell yield, improved control of plasma parameters for high energy density experiments and better ability to model and predict performance for existing and future devices.

One potential method for reducing MRT growth is to adjust the initial density distribution so that the unstable interface between the plasma and magnetic field has reduced (or zero) acceleration. For a radially-extended initial density profile, i.e., not a narrow annular shell, the current sheet "snow plows" through the gas. For high enough Z, the sheath remains cool and narrow due to radiation and accretes mass as it implodes. The reduced MRT drive comes at the cost of losing approximately 50% of the sheath kinetic energy to radiation during the run-in.

We can use simple OD force balance arguments to derive the shape of a profile with constant implosion velocity. The force equation gives

$$\frac{L'I^2}{2} = \dot{M}v \qquad (6)$$

where $L' = \frac{\mu_0}{2\pi}\frac{l}{r}$ is the radial rate-of-change of the inductance and $\dot{M} = 2\pi l \rho v$ is the mass snowplow rate. Given a current versus time we can solve Eq.(6) for the density:

$$\rho(r) = \frac{\mu_0 I^2}{8\pi^2 r^2 v^2} \tag{7}$$

where I(t) is evaluated at $t = (r_0 - r)/v$. For SATURN, we know the drive voltage rather than the current. If we model the driving circuit as a voltage source, V(t), in series with a resistor, R (R = 1/6 ohm for SATURN) , an external inductor, L_{ext}, and the imploding plasma, then the current can be found from

$$I(t) = \frac{1}{L}\exp\left(-\int^{t}\frac{R}{L}dt'\right)\int^{t}V(t')\exp\left(\int^{t'}\frac{R}{L}dt''\right)dt' \tag{8}$$

where $L = L_{ext} + \frac{\mu_0 l}{2\pi}\ln\left(\frac{r_0}{r}\right)$. For a given drive voltage waveform, resistance and external inductance, the profiles from Eq.(7) are parametrized by the velocity, v and initial radius, r_0. For efficient coupling we need to match the implosion time with the driver, e.g., choose r_0 / v equal to the time of positive drive voltage (80 ns for SATURN). Fig.(8) shows the constant velocity density profiles for the SATURN drive waveform with L_{ext}= 11 nH, r_0 / v = 80 ns and two different implosion velocities.

1D simulations of krypton implosions with a profile corresponding to a constant velocity of 5 x 10^7 cm/s confirm that the sheath remains narrow and moves in at the expected, unvarying speed. We have also done 2D simulations with a 1% random density perturbation and periodic

boundary conditions modeling 1/10 of a total pinch length of 2 cm. The implosion still shows significant 2D behavior, possibly as a result of residual curvature-driven instability or Richtmeyer-Meshkov instability of the snowplow shock front. A slight deceleration of the sheath might compensate for the curvature driven instability. The simulation output power is enhanced, however, in comparison with experiments or 2D modeling of annular loads. The output power exceeds 80 TW with 30 TW greater than 1 keV, as shown in Fig.(9).

A possible method for generating these profiles is to embed a solid wire in a gas puff peaked on axis. The wire will heat and expand under the influence of the x-rays produced during the sheath run-in, creating a profile resembling Fig.(8). Also, deviations from the profile within a radius ~ mm will probably not degrade performance appreciably.

V. CONCLUSIONS

2D radiation MHD calculations indicate that MRT modes should grow to large amplitude and determine the x-ray output pulse widths for a variety of SATURN loads. The code predicts x-ray output times and magnitudes in approximate agreement with experiments, although the simulations over-predict the density near r = 0. Relatively weak 3D effects could reduce the peak density significantly since the mass near the origin has undergone a large radial convergence, although anomalous resistance

or the Hall effect may also play a role. In the run-in phase where the instability develops, we find that experimental x-ray images show ring-like structures similar to those predicted by the 2D model. Finally, we have derived profiles that should be less susceptible to MRT modes and modeled an example driven by SATURN. The simulated implosion produced several times the peak power observed for other loads.

ACKNOWLEDGMENTS

The authors acknowledge useful discussions with George Allshouse, Chris Deeney, Kent Estabrook, Charles Hartman, Keith Matzen, Steve Maxon, Albert Osterheld, Rick Spielman and Brian Wilson. This work performed under the auspices of the U.S. Department of Energy by Lawrence Livermore National Laboratory under Contract No. W-7405-ENG-48.

REFERENCES

[1] D.D. Bloomquist, R.M. Stinnett, D.H. McDaniel, J.R. Lee, A.W. Sharpe, J.A. Halbleib, L.G. Shlitt, P.W. Spence and P. Corcoran, *Proc. 6th IEEE Pulsed Power Conference*, Arlington, VA, ed. P.J. Turchi and B.H. Bernstein (IEEE, New York, 1987), p. 310.

[2] K.L. Wong, P.T. Springer, J.H. Hammer, A. Osterheld and C. Deeney, Bull. Am. Phys. Soc.,8T44,(1995).

[3] T.W.L. Sanford, T.J. Nash, B.M. Marder, R. Humphreys, C. Deeney, R.B. Spielman, J.F. Seamen, R.C. Mock, J.S. McGurn, D. Jobe, T.L. Gilliland, M. Vargas, K. Struve, W.A. Stygar, J.H. Hammer, J.L. Eddleman, J.S. DeGroot, D. Mosher, K.G. Whitney, J.P. Apruzese, P. Pulsifer, Y. Maron, Bull. Am. Phys. Soc., 8R02,(1995).

[4] T.W. Hussey, N.F. Roderick, and D.A. Kloc, J. Appl. Phys. **51**,1452 (1980).

[5] J.H. Hammer,J.L Eddleman, J.S. DeGroot, M. Tabak, A. Toor and G.B. Zimmerman,Bull. Am. Phys. Soc. (1994).

[6] T.W. Hussey, N.F. Roderick, U. Shumlak, R.B. Spielman and C.Deeney, Phys. Plasmas **2**,2055(1995).

[7] R.B. Spielman, D.L. Hanson, M.A. Palmer, M.K. Matzen, T.W. Hussey, and J.M. Peek, J. Appl. Phys. **57**, 883 (1985).

[8] W.Hsing (private communication, 1989).

[9] J.L. Eddleman, J.S. DeGroot, R.B. Spielman, C.W. Hartman. M.Gee, J.H. Hammer,K.G. Estabrook, W.B. Bateson and D.W. Hewett, Bull. Am. Phys. Soc. ,8R13 (1995)

[10] N.F. Roderick and T.W. Hussey, J. Appl. Phys. **56**, 1387 (1984).

[11] T.W. Husse and N.F. Roderick, Phys. Fluids **24**,1384 (1981).

[12] W. A. Lokke and W.H. Grassberger, "Xsnq-u, A Non-lte Emission and Absorption Coefficient Subroutine," Lawrence Livermore National Laboratory Rept., UCRL-52276, 1977.

[13] R.M. More, K.H. Warren, D.A. Young and G.B. Zimmerman, Phys. Fluids ,**31**, 3059 (1988).

[14] Y.T. Lee and R.M. More, Phys. Fluids **27**, 1273 (1984).

FIGURE CAPTIONS

Fig.(1) Imploding z-pinch configuration.

Fig.(2) Density profile in an accelerated reference frame.

Fig.(3) X-ray output power per unit solid angle measured by the bolometer for shot 2094 in TW/sr, compared with simulations: A, a single mode density perturbation with amplitude 1% and wavelength 1 mm; B, a 1% random initial density perturbation with periodic boundary conditions and simulation length of 2 mm; C, a 5% random density perturbation with periodic boundary conditions and simulation length of 1 mm.

Fig.(4) X-ray framing camera image (width at source = 1.2 cm) of an imploding neon-argon solid gas puff 3 ns before stagnation. The z-axis is vertical and the view angle is 65° from the z-axis. The shadow of the anode wires is visible.

Fig.(5) Density contours from a simulation of neon-argon gas puff at t = 67 ns. The peak value is 3.2×10^{-4} g/cc. The initial puff density is 9×10^{-6} g/cc.

Fig.(6) Post-processed image (width at source = 1.2 cm) of keV x-ray emission from neon-argon simulation at t = 67 ns. The z axis is vertical and the view angle is 65° from the z-axis.

Fig.(7) X-ray framing camera image (width at source = 1.2 cm) of an imploding neon-argon solid gas puff at time similar to Fig.(5). The z axis is vertical and the view angle is 65° from the z-axis.

Fig.(8) Density vs. radius for improved stability profiles.

Fig.(9) Output power vs. time for 2D krypton improved stability profile.

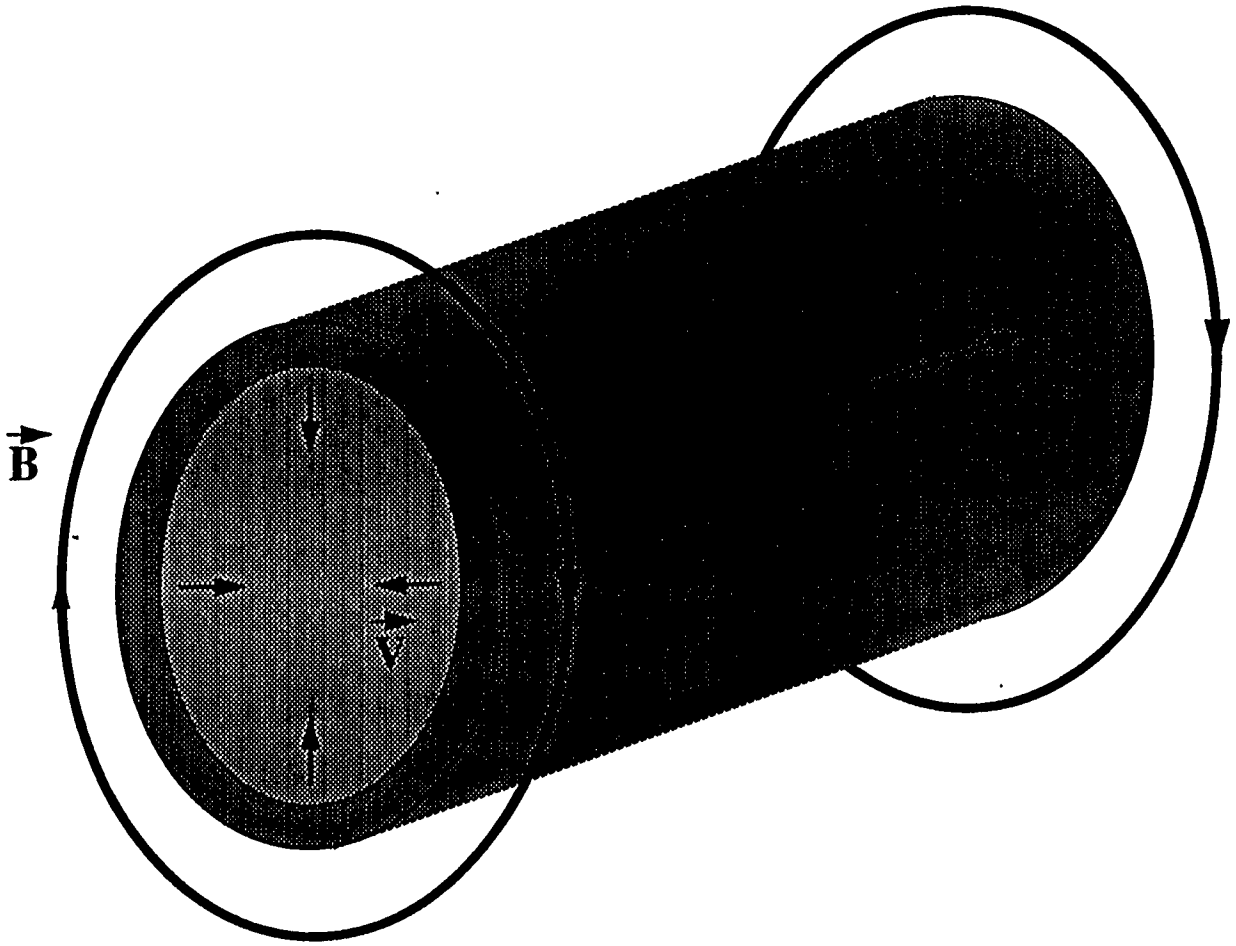

Fig. 1, Hammer,et.al., Phys. Plasmas

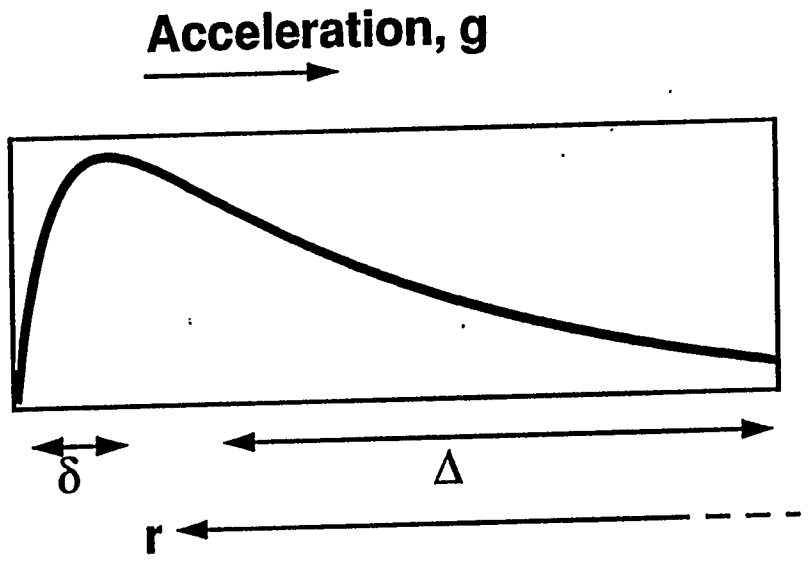

Fig. 2 Hammer,et.al., Phys. Plasmas

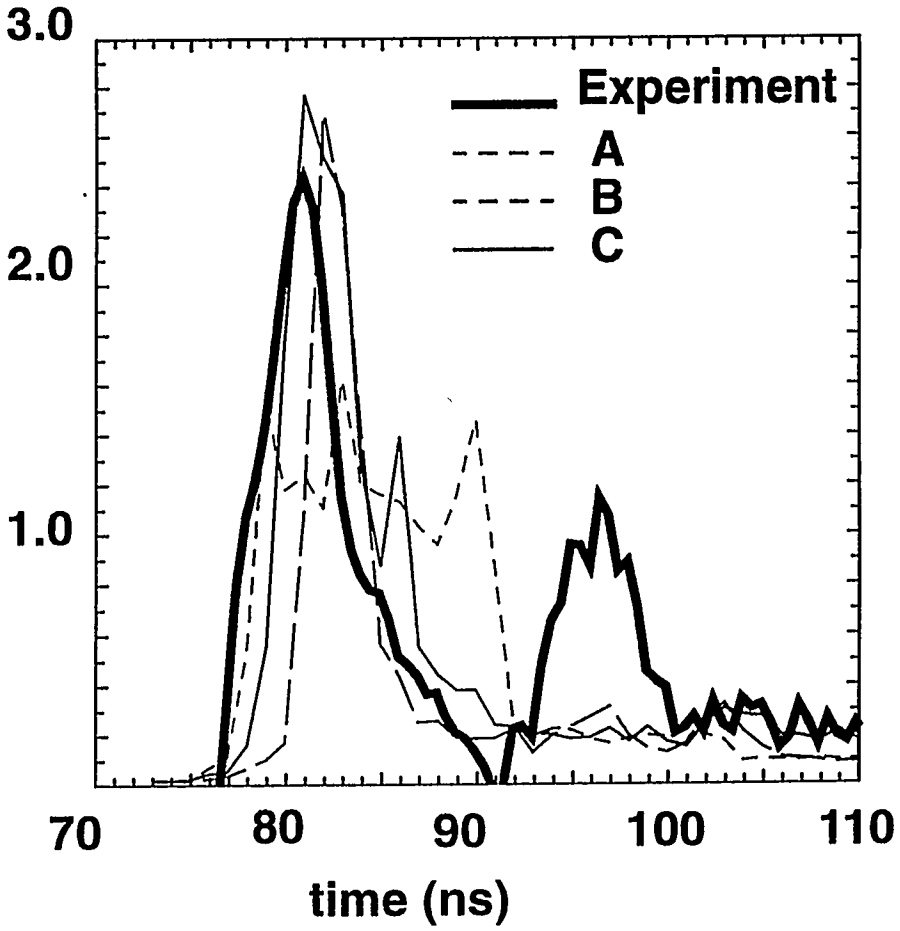

Fig. 3, Hammer, et.al., Phys. Plasmas

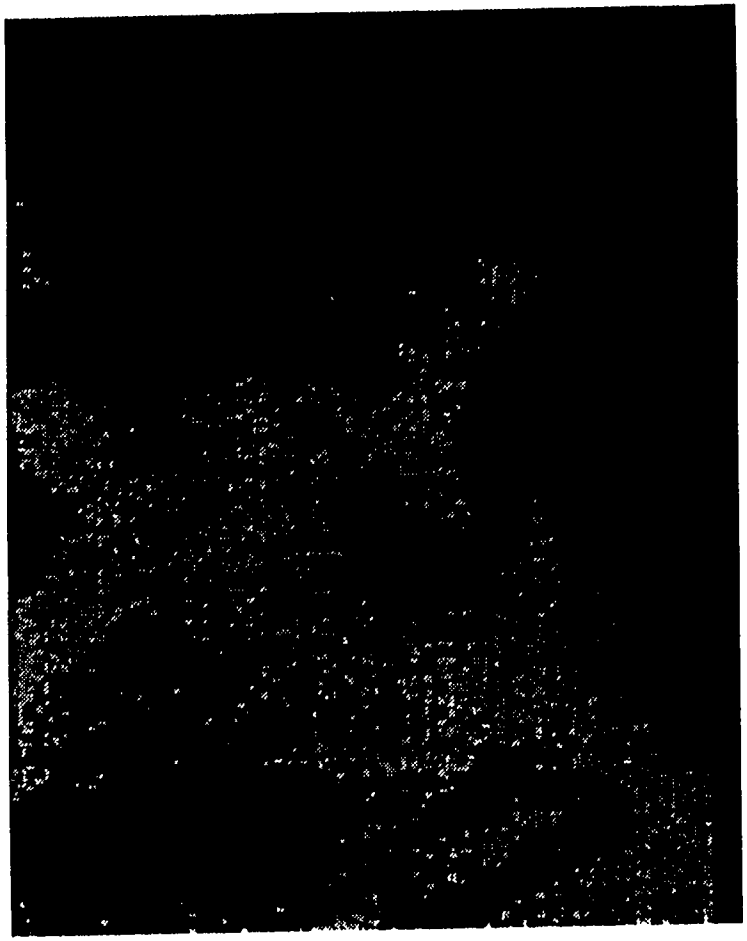

Fig. 4 , Hammer,et.al., Phys. Plasmas

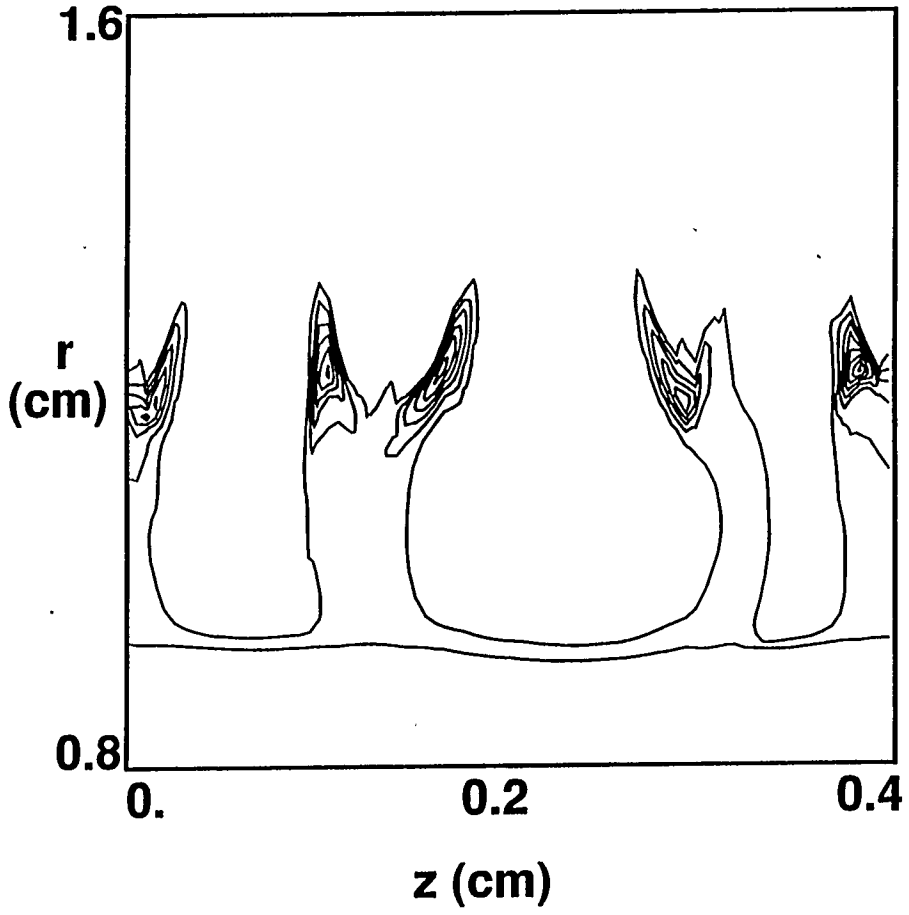

Fig. 5, Hammer, et. al., Phys. Plasmas

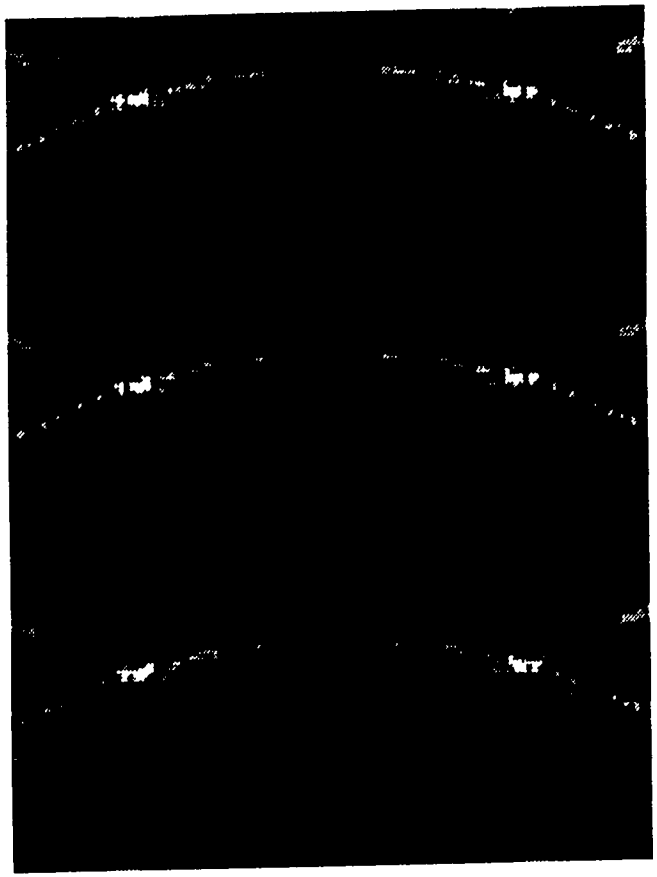

Fig. 6, Hammer,et.al., Phys. Plasmas

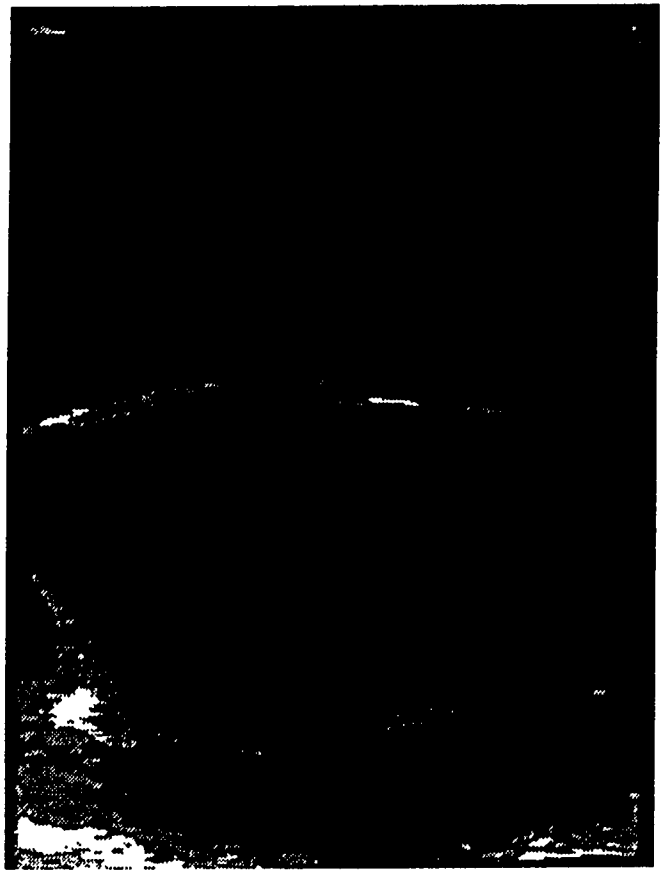

Fig. 7, Hammer,et.al., Phys. Plasmas

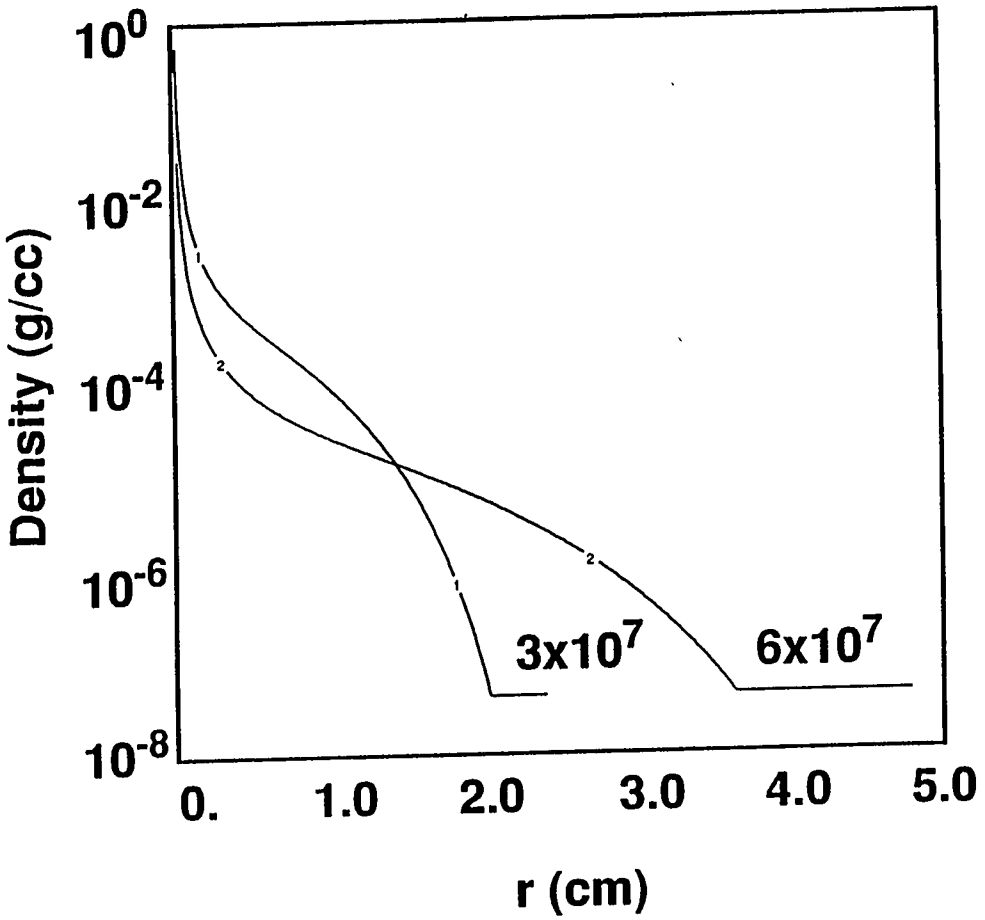

Fig. 8, Hammer,et.al. , Phys. Plasmas

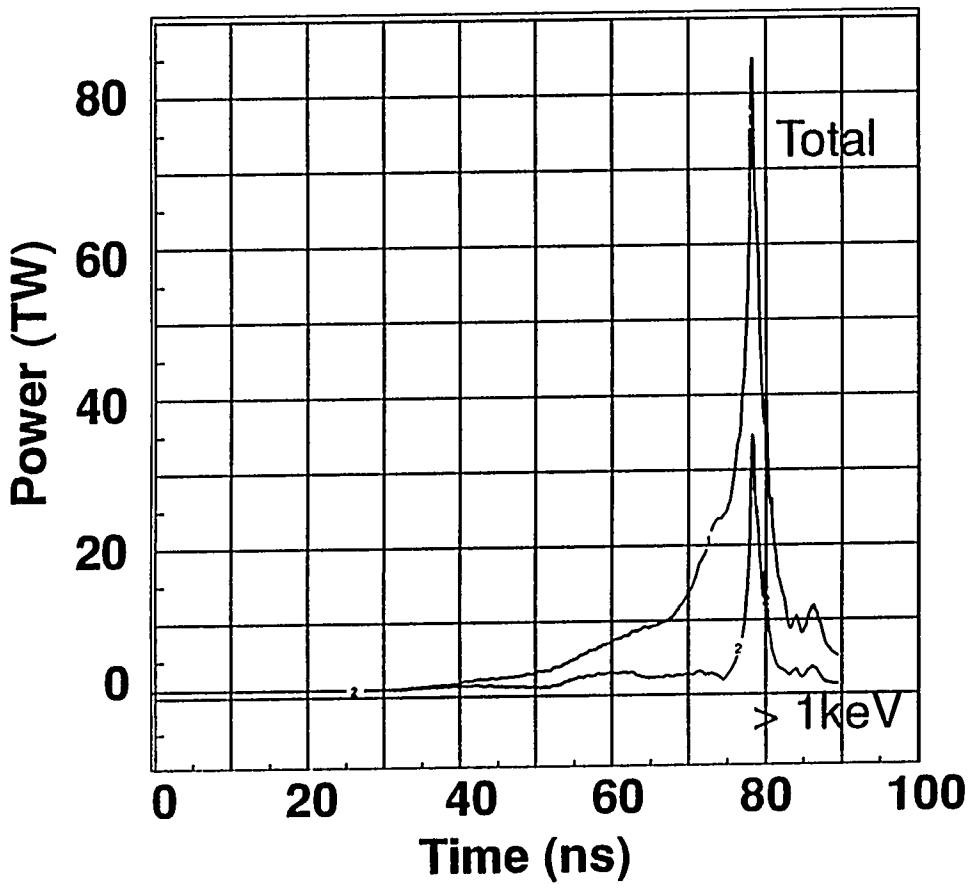

Fig. 9 Hammer et al. Phys. Plasmas

Technical Information Department • Lawrence Livermore National Laboratory
University of California • Livermore, California 94551